ACS Catalysis

Research Article

pubs.acs.org/acscatalysis

Influence of the Reaction Temperature on the Nature of the Active and Deactivating Species During Methanol-to-Olefins Conversion over H-SAPO-34

E. Borodina,[†] H. Sharbini Harun Kamaluddin,[†,‡] F. Meirer,[†] M. Mokhtar,[‡] A. M. Asiri,[‡] S. A. Al-Thabaiti,[‡] S. N. Basahel,[‡] J. Ruiz-Martinez,*[,†] and B. M. Weckhuysen*[,†]

[†]Inorganic Chemistry and Catalysis, Debye Institute for Nanomaterials Science, Utrecht University, Universiteitsweg 99, Utrecht 3584 CG, The Netherlands

[‡]Department of Chemistry, King Abdulaziz University, P.O. Box 80203, Jeddah 21589, Saudi Arabia

Supporting Information

ABSTRACT: The selectivity toward lower olefins during the methanol-to-olefins conversion over H-SAPO-34 at reaction temperatures between 573 and 773 K has been studied with a combination of operando UV−vis diffuse reflectance spectroscopy and online gas chromatography. It was found that the selectivity toward propylene increases in the temperature range of 573−623 K, while it decreases in the temperature range of 623−773 K. The high degree of incorporation of olefins, mainly propylene, into the hydrocarbon pool affects the product selectivity at lower reaction temperatures. The nature and dynamics of the active and deactivating hydrocarbon species with increasing reaction temperature were revealed by a non-negative matrix factorization of the time-resolved operando UV−vis diffuse reflectance spectra. The active hydrocarbon pool species consist of mainly highly methylated benzene carbocations at temperatures between 573 and 598 K, of both highly methylated benzene carbocations and methylated naphthalene carbocations at 623 K, and of only methylated naphthalene carbocations at temperatures between 673 and 773 K. The operando spectroscopy results suggest that the nature of the active species also influences the olefin selectivity. In fact, monoenylic and highly methylated benzene carbocations are more selective to the formation of propylene, whereas the formation of the group of low methylated benzene carbocations and methylated naphthalene carbocations at higher reaction temperatures (i.e., 673 and 773 K) favors the formation of ethylene. At reaction temperatures between 573 and 623 K, catalyst deactivation is caused by the gradual filling of the micropores with methylated naphthalene carbocations, while between 623 and 773 K the formation of neutral poly aromatics and phenanthrene/anthracene carbocations are mainly responsible for catalyst deactivation, their respective contribution increasing with increasing reaction temperature. Methanol pulse experiments at different temperatures demonstrate the dynamics between methylated benzene and methylated naphthalene carbocations. It was found that methylated naphthalene carbocations species are deactivating and block the micropores at low reaction temperatures, while acting as the active species at higher reaction temperatures, although they give rise to the formation of extended hydrocarbon deposits.

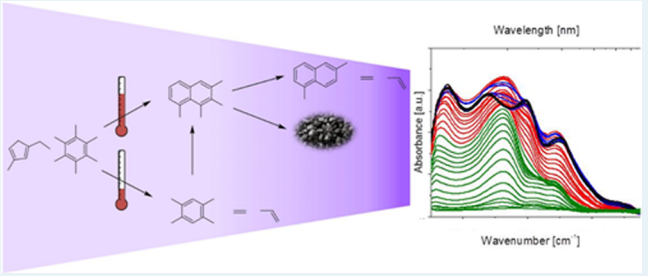

KEYWORDS: *methanol-to-olefins, zeolites, operando, UV−vis spectroscopy, active species, deactivation, chemometrics*

1. INTRODUCTION

The conversion of methanol into olefins (MTO) can be performed using different types of heterogeneous acid-based catalyst materials, such as microporous aluminosilicates and silicoaluminophosphates.[1−6] The MTO process and related catalyst materials have been intensively studied since the 1970s. The synthesis of light olefins, such as ethylene and propylene, has attracted a lot of attention as they are the key intermediates for the production of many useful chemicals and polymers. Ethylene is used for the preparation of polyethylene, ethylene oxide, styrene, ethylene glycol, and polyvinyl chloride, while propylene is an important base chemical for the production of propylene oxide, phenol, and polypropylene, for example.

The MTO reaction is a highly complex process. Understanding and elucidating the reaction mechanism is challenging and has implications for both fundamental research and commercial application. Among the proposed mechanism for the MTO reaction, the most generally accepted is the one proposed by Dahl and Kolboe.[7] It involves the formation of a hydrocarbon pool (HCP), but it only explains the autocatalytic part of the MTO reaction.

Received: May 7, 2017
Revised: June 21, 2017
Published: July 12, 2017

DOI: 10.1021/acscatal.7b01497
ACS Catal. 2017, 7, 5268−5281

According to few recent studies, the MTO reaction is initiated by hydrocarbon species, like acetate/formate, methyl acetate, and dimethoxymethane, which were formed during the very early stages of reaction.[8−11] All these species eventually participate in the formation of HCP species during the course of reaction. On the other hand, large and systematic efforts have already been devoted to elucidate the HCP mechanism of MTO reaction using a wide variety of theoretical[9,12−14] and experimental approaches.[8−11,15−31] From the experimental point of view, next to kinetic and isotopic labeling experiments,[15−18] several spectroscopic techniques, such as solid-state NMR,[9,11,19−23] UV−vis, fluorescence (micro)spectroscopy,[24−28] and FT-IR (micro)spectroscopy[29−31] have been used. On the basis of these findings, methylated benzene carbocations[32] and cyclopentenyl carbocations[33] are generally accepted as the active hydrocarbon pool species during the zeolite-catalyzed MTO process, including both H-ZSM-5 and H-SAPO-34 molecular sieves. For example, Haw et al. correlated the product selectivity during the MTO process with the nature of the hydrocarbon pool species formed in SAPO-34 zeolite pores using a combination of GC analysis with pulse-quench in situ NMR.[34] They observed that methylated benzenes with five or six methyl groups per ring are the most active for olefins formation with a higher selectivity toward propylene than toward ethylene. In contrast, methylated benzenes with fewer methyl groups (i.e., ∼3 $-CH_3$) were less active, but showed a higher selectivity toward ethylene.

Furthermore, there are other factors, such as catalyst acidity and coke content, which affect the product selectivity. Formation of coke inside the zeolite material also causes changes in the material properties. It might for example influence the density and strength of acid sites and cavity size, which lead to different product selectivity and nature of intermediate species. For example, Chen et al. studied the relation between coke formation and selectivity.[35] They observed that selectivity changes with the amount of coke less than 10 wt % were independent of the zeolite crystal size. In particular, the selectivity toward ethylene increases with increasing coke content. Furthermore, it was found that the propylene/ethylene molar ratio decreased with increasing coke content, but was independent of the crystal size up to 12 wt % of coke.[36] Wang et al. observed that the selectivity toward ethylene and propylene over SAPO-34 does not depend only on the catalyst structure, but it is also influenced by the reaction conditions.[12] They proposed a reaction network, where cracking reactions play a key role in the product selectivity. From their calculations, ethylene is produced via cracking of C_5^+ and C_6^+ ions with higher barriers, while propylene is produced via cracking of higher enyl carbocations.

In addition, Lercher and co-workers performed the methanol-to-olefins reaction accompanied by cofeeding aromatic or olefins in order to understand the product selectivity.[37] For this purpose, various aromatic molecules (i.e., benzene, toluene, and xylene) or olefins (i.e., ethylene, propylene, 1-butylene, 1-pentene, and 1-hexene) were used as cofeeding components during the methanol-to-olefins reaction over H-ZSM-5. The addition of aromatic molecules (16−32 C%), which enhanced the aromatics-based catalytic cycle and greatly suppressed the olefin-based cycle, leads to an enhanced formation of methane and ethylene accompanied by the methylation of aromatic rings at the expense of propylene and C_4^+ higher olefins. The ratio of propylene to ethylene is controlled by the concentration of the added aromatic molecules.[37] Wu et al. studied the effect of adding ethylene, propylene, and water to methanol feed during the MTO reaction over H-SAPO-34.[38] They observed that when propylene is fed with methanol and water, the selectivity toward propylene decreases, but the selectivity toward ethylene and $C_4^=$ olefins increases. Interestingly, when ethylene is fed to a reactor, the selectivity toward ethylene decreases, but the selectivity toward propylene and butenes increases. These results indicate that ethylene and propylene react with methanol to form propylene and $C_4^=$ olefins, respectively. The presence of propylene in the feed inhibits the reaction of ethylene with methanol through competition for the adsorption on a stronger acidic site.[38] Corma and co-workers have studied the H-SAPO-34 and found that silicon distribution strongly affects the lifetime and product selectivity.[39] They observed that a higher C_2/C_3 ratio is related to a higher population of Si atoms at the border of the Si islands, which are considered to be the acid sites of higher strength.

From the above discussions, it becomes evident that various parameters affect the selectivity toward ethylene and propylene during the MTO process. More specifically, the factors include the nature of the reaction intermediate species formed,[34] the size of the cavity and the related type of zeolite structure,[40,41] the formation of coke within cavity,[35] the crystal size of zeolite materials,[39] the acid site density,[35,39] and the reaction conditions, such as space velocity[42] and reaction temperature.[43] On the other hand, there are a limited number of papers, which provide a detailed explanation of the reasons for the propylene-to-ethylene selectivity change within a specific parameter, including for example the reaction temperature.

In this work, the MTO conversion process has been studied in detail over H-SAPO-34 at different reaction temperatures (i.e., between 573 and 773 K). By using a combination of operando time-resolved UV−vis diffuse reflectance spectroscopy and online gas chromatography, it becomes possible to determine the reasons for the variation of product composition with increasing reaction temperatures. This work is complementary to a recent study from our group focusing on the influence of the reaction temperature on the nature of the active and deactivating species during the MTO process over zeolite H-SSZ-13.[28] As a result, a detailed comparison can be made between the reaction and deactivation behavior of H-SAPO-34 and H-SSZ-13 for different reaction temperatures. Furthermore, by using methanol pulse experiments at different temperatures, we can determine the dynamics of different hydrocarbon pool species, and their relative contributions to the formation of ethylene and propylene, as well as catalyst deactivation.

2. EXPERIMENTAL SECTION

2.1. Characteristics of H-SAPO-34. The H-SAPO-34 catalyst under study was purchased from ACS Material (U.S.A.). The catalyst sample was calcined in air under the following conditions: 1 K·min^{-1} to 393 K, held for 2.5 h; 2.2 K·min^{-1} to 623 K, and held for 3 h; and finally 0.8 K·min^{-1} to 853 K, and held for 3 h. After calcination, the catalyst material was in its H-form. The crystal size and morphology were determined by scanning electron microscopy (SEM), using a Tecnai FEI XL 30SFEG instrument, while the overall crystallinity was measured by a Bruker D2 X-ray powder diffractometer equipped with a Co Kα X-ray tube (λ = 1.7902 Å). The X-ray diffraction (XRD) pattern was recorded in the region of 5° - 50° 2θ at room temperature. The sample acidity was measured with temperature-programmed desorption (TPD) of ammonia using a Micrometrics AutoChem 2910 apparatus. Prior to ammonia TPD, 100 mg of sample were placed in a quartz tube reactor and

DOI: 10.1021/acscatal.7b01497
ACS Catal. 2017, 7, 5268−5281

preheated at 823 K in 25 mL·min^{-1} of He flow for 30 min. Adsorption of ammonia (5 vol % in He) was performed for 45 min at 373 K. The physisorbed ammonia was flushed under a He stream (50 mL·min^{-1}) at 373 K for 2 h. After that, the ammonia TPD was carried out in a He flow at the range of temperatures of 373 to 873 K using a heating rate of 10 K·min^{-1}. The amount of adsorbed ammonia was measured by a thermal conductivity detector (TCD). The pore volume and surface area were determined by Ar physisorption measurements using a Micromeritics ASAP 2420.

2.2. Operando UV−vis Diffuse Reflectance Spectroscopy. Catalytic testing was done in a fixed-bed quartz reactor. The catalyst powder was pressed into a pellet and then was crushed and sieved. The 212−425 μm fraction was used for the catalytic tests. Prior to the reaction, ∼50 mg of the catalyst were activated at 823 K under 100% oxygen for 1 h and then cooled down to the desired reaction temperature. Weight-hourly space velocity (WHSV) of methanol was kept at 0.5 g·g^{-1}·h^{-1} by flowing He gas through a methanol saturator, which was kept at 293 K. The catalytic reactions were performed at a wide range of temperatures, 573−773 K, where the catalyst was fully active for the MTO reaction. For the analysis of the reactant and reaction products, online gas chromatography (GC) was performed using an Interscience Compact GC instrument equipped with Rtx-1+Rtx-Wax, Rt-TCEP+Rtx-1 and Al_2O_3/Na_2SO_4 columns, and a TCD and two flame ionization detectors (FIDs). Olefins/water feeding experiments were carried out in the same setup and conditions as the MTO catalytic testing. Instead of methanol, a mixture of ethylene, propylene, and water was flowed through the H-SAPO-34 catalyst at 573, 598, 623, 673, and 773 K. The olefins were flowed using mass flow controllers, and water was introduced using a saturator in a similar way as the methanol experiments. The WHSV of ethylene, propylene, and water were 0.23, 0.23, and 0.14 g·g^{-1}·h^{-1}, respectively, which gives a total WHSV of 0.6 g·g^{-1}·h^{-1}.

The nature and dynamics of the hydrocarbon pool active species and related coke compounds formed during the MTO and olefin reactions were investigated by operando UV−vis diffuse reflectance spectroscopy. A UV−vis light was focused into the whole reactor bed using a custom-made Avantes high-temperature UV−vis probe. This probe comprises one excitation and one collection optical fiber with 400 μm diameter and 1.5 m length. The optical fibers are placed in a stainless steel protection sleeve, which is specially designed to operate under reaction temperatures up to 873 K. The UV−vis probe is connected to a deuterium-halogen light source and the UV−vis light, ranging between 12 500 cm^{-1} and 45 000 cm^{-1}, was collected by an AvaSpec 2048 UV−vis spectrometer. Operando UV−vis diffuse reflectance spectra were collected every 30 s, with 100 accumulations of 140 ms exposure time each. These settings ensure an appropriate signal-to-noise ratio with an adequate time resolution to monitor the dynamics of the UV−vis spectra. A detailed scheme of the operando UV−vis spectroscopy-online GC set up, as well as other characteristics of the setup can be found in a previous publication from our group.[28]

For the analysis of the time-resolved operando UV−vis diffuse reflectance spectroscopy data, non-negative matrix factorization (NNMF) was applied. NNMF[44,45] is a widely used factor analysis method to factorize a (non-negative) data matrix T × W into two matrices X (T × k) and Y (k × W) with the constraints that all matrices have only positive elements. Detailed information about the application of NNMF in the treatment of the operando UV−vis diffuse reflectance spectra can be found in our previous publication on the catalytic and spectroscopic properties of zeolite H-SSZ-13.[28]

2.3. Methanol-to-Olefins Quenching Experiments. The same operando UV−vis diffuse reflectance spectroscopy set up was used to perform experiments where the MTO reaction was quenched. The catalyst preparation and reaction conditions were the same as for a typical MTO experiment. The first experiment includes the start of the methanol flow at 523 K, heating the H-SAPO-34 material up to 543 K and holding it at this temperature while flowing methanol. After that the methanol flow was stopped, and the catalyst was flushed with He until no methanol and reaction products were detected by online GC. The final stage involves heating the H-SAPO-34 material up to 573 K, holding it at this temperature and cooling down to room temperature. The second experiment was performed in the same manner. The temperature was 573 K when the methanol flow started. The catalyst was heated up to 623 K and held at this temperature until no products and methanol were detected. Subsequently, the reactor was cooled to room temperature.

3. RESULTS AND DISCUSSION

3.1. Catalyst Characterization. The XRD pattern of the calcined H-SAPO-34 catalyst, shown in Figure S1a, indicates that the sample has the chabazite (CHA) structure. More specifically, the XRD pattern includes the characteristic reflections of this framework structure, that is, at 2θ 11.3, 15.3, 16.5, 19.0, 21.0, 22.6, 24.4, 27.3, 29.5, 30.7, 36.2, 36.8, as reported by the International Zeolite Association.[46] The peak at ∼10° 2θ does not correspond to the presence of an additional phase in the sample and it arises from the CHA reflection of the Co anode Kβ line. This line contributes to the H-SAPO-34 X-ray pattern and is present because of the XRD diffractometer used, which does not filter out all the Co Kβ lines. A detailed explanation of this instrumental issue is provided in our earlier publication.[28] Crystal sizes of the material, as determined by SEM, range between 1 and 8 μm, as shown in the micrograph in Figure S1b. The ammonia TPD profile of the sample is reported in Figure S1c. The H-SAPO-34 material contains weak and strong acid sites, which correspond to the TPD peaks at low (420 K) and high temperatures (600 K).[47] The desorption band at 420 K can be assigned to ammonia adsorbed either on physically[48] or weak Lewis acid sites.[49] The ammonia desorbed at higher temperatures (i.e., 620 K for the H-SAPO-34 under investigation) is related to the number of strong Brønsted acid sites (BAS).[50] These measurements revealed that the amount of desorbed ammonia at high temperature is 0.5 mmol·g^{-1}. Considering that the amount of silicon in the samples is 1.9 mmol·g^{-1}, 27% of the silicon atoms are creating Brønsted acid sites. Ar adsorption and desorption isotherms are shown in Figure S2. The material has a BET surface area of 530 m^2·g^{-1} and is fully microporous, with a micropore volume of 0.15 cm^3·g^{-1}.

3.2. Catalytic Performance. We have recently reported a relationship between the hydrocarbon species formed inside a H-SSZ-13 zeolite catalyst and its activity and deactivation.[28] Additionally, it was found that the reaction temperature influences the rate and nature of the hydrocarbon species inside the catalyst and its catalytic performance. Our first scientific question is now if we can find a similar relationship for a H-SAPO-34 material, which is structurally analogous to zeolite H-SSZ-13 (CHA framework). The catalytic performance of H-SAPO-34 was first evaluated at different MTO reaction temperatures (i.e., 573, 598, 623, 679, and 773 K) using a

DOI: 10.1021/acscatal.7b01497
ACS Catal. 2017, 7, 5268−5281

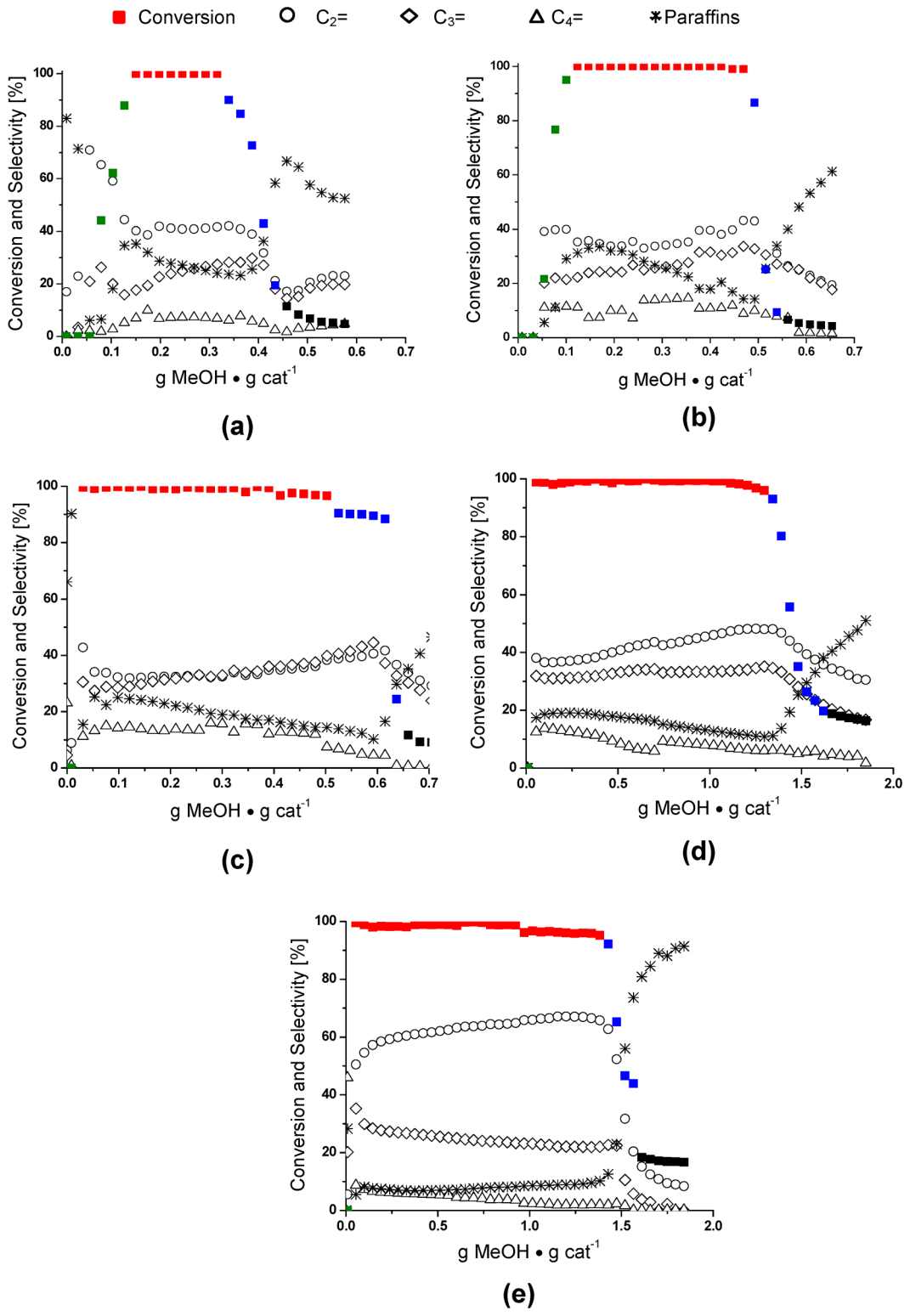

Figure 1. Conversion and selectivity profiles for the methanol-to-olefin reaction as a function of methanol throughput over H-SAPO-34 at a WHSV of 0.5 $g{\cdot}g^{-1}{\cdot}h^{-1}$ at (a) 573 K; (b) 598 K; (c) 623 K; (d) 673 K; and (e) 773 K. The green points correspond to the induction period, when conversion of methanol is less than 100%; the red points indicate a period of full conversion of methanol; the blue points relate to the deactivation period, when the conversion of methanol drops from 100% to 20%; while the black points correspond to the deactivated catalyst, when the conversion of methanol is less than 20%.

WHSV of 0.5 $g{\cdot}g^{-1}{\cdot}h^{-1}$. The conversion and selectivity as a function of the methanol throughput are presented in Figure 1.

By evaluating the catalytic conversion, for all the reaction temperatures, the H-SAPO-34 sample shows an induction period where no catalytic activity is observed. This induction period could be attributed to the existence of a direct mechanism, which is operational just prior to the HCP mechanism, during the early stages of the MTO reaction. Methanol is initially consumed in

DOI: 10.1021/acscatal.7b01497
ACS Catal. 2017, 7, 5268−5281

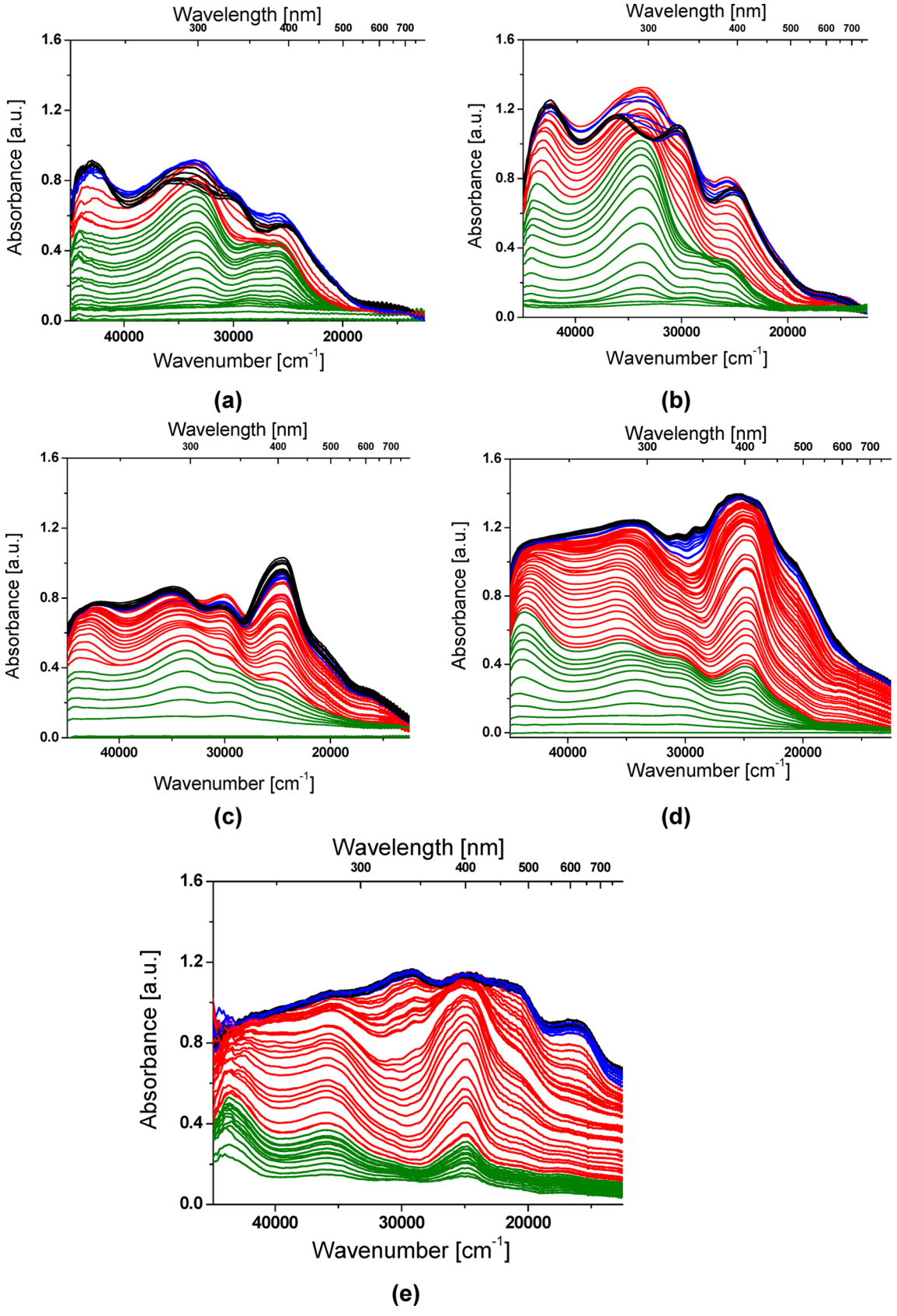

Figure 2. Time-resolved operando UV−vis diffuse reflectance spectra recorded for the methanol-to-olefin reaction over the H-SAPO-34 material at a WHSV of 0.5 $g \cdot g^{-1} \cdot h^{-1}$ at (a) 573 K; (b) 598 K; (c) 623 K; (d) 673 K; and (e) 773 K. The green spectra correspond to the induction period, when conversion of methanol is less than 100%; the red spectra indicate a period of full conversion of methanol; the blue spectra relate to the deactivation period, when the conversion of methanol drops from 100% to 20%; while the black spectra correspond to the deactivated catalyst, when the conversion of methanol is less than 20%.

DOI: 10.1021/acscatal.7b01497
ACS Catal. 2017, 7, 5268−5281

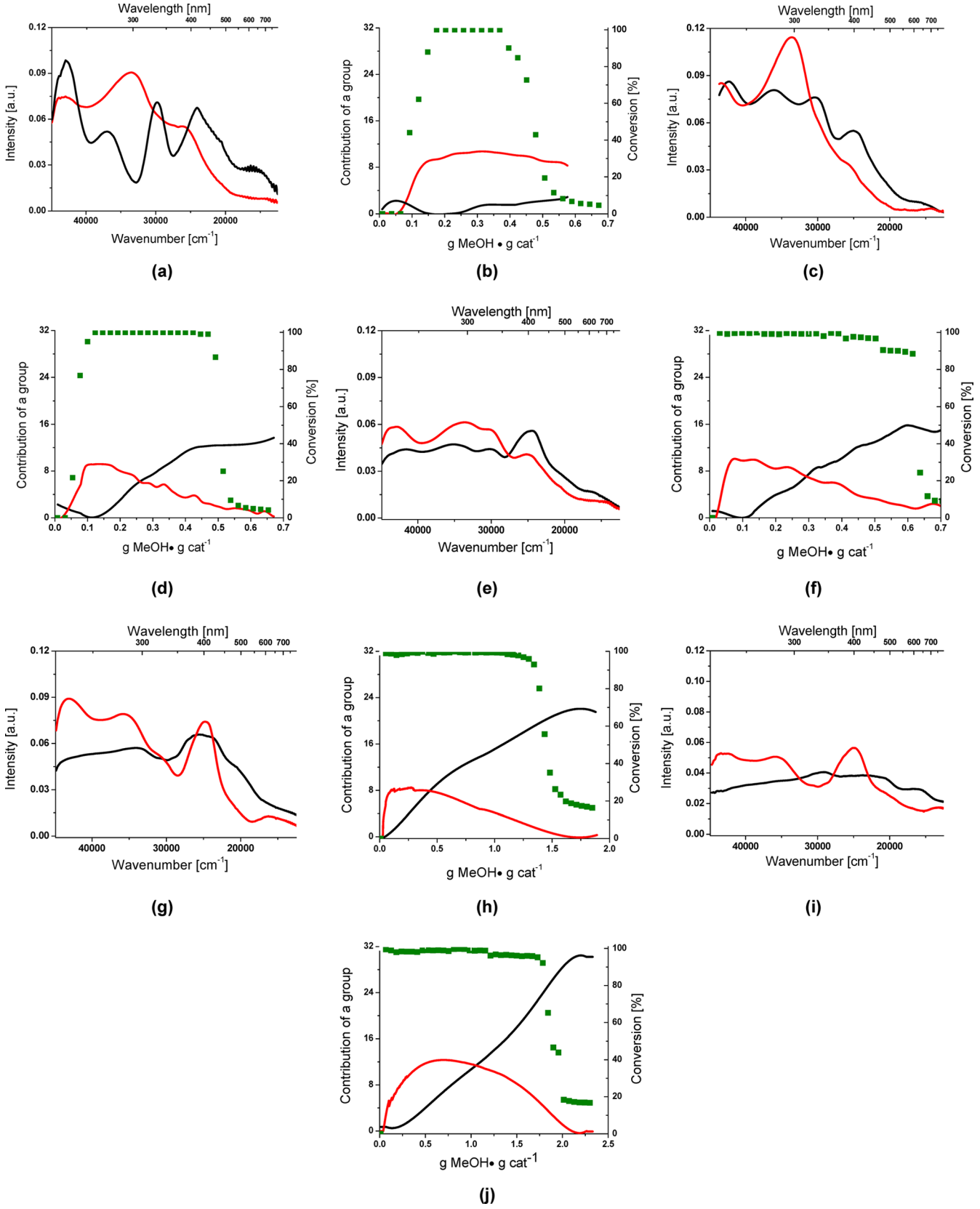

Figure 3. Non-negative matrix factorization of the time-resolved operando UV−vis diffuse reflectance spectroscopy data. The operando UV−vis spectra during methanol-to-olefins (MTO) reaction over H-SAPO-34 were deconvoluted into two groups of absorption bands (eigenspectra) for the hydrocarbon species with different kinetics (a, c, e, g, i) and the evolution of every group of hydrocarbon species as a function of methanol loading on the catalyst material (b, d, f, h, j). The spectra were recorded during the MTO reaction at 573 K (a and b), 598 K (c and d), 623 K (e and f), 673 K (g and h) and 773 K (i and j). The red curve represents group I (active hydrocarbon species), while the black curve corresponds to group II (deactivating hydrocarbon species). The green dots in the figures correspond to the values for catalytic conversion.

DOI: 10.1021/acscatal.7b01497
ACS Catal. 2017, 7, 5268−5281

the formation of zeolite acetate/formate, methyl acetate, and dimethoxymethane as a result of "methanol decarbonylation/zeolite carbonylation" pathway during induction period of MTO reaction.[8−11] All these species formed during the induction period later initiate and/or participate in the formation of HCP species during the course of MTO reaction, as has recently been observed independently by Lercher and co-workers[10] and our research group.[11] This induction period is particularly pronounced for low reaction temperatures (i.e., 573 and 598 K). During this typical period in the MTO reaction, the active hydrocarbon species for this process are forming inside of the H-SAPO-34 nanocages.[51]

The catalyst lifetime increases with increasing reaction temperature, within the range of temperatures studied (i.e., 573−773 K). Our results do not correlate with previous studies by Bleken et al.,[51] where the optimum reaction temperature was 673 K. It is important to mention that we were also unable to correlate our previous results on H-SSZ-13[28] with those reported by Bleken et al.[51] Intrigued by this divergence in results, we have checked the temperature in the reactor with a second thermocouple and found that the temperature could only deviate ∼25 K, which does not explain the observed differences. In this way, one could think that other parameters, for instance, particle size and acidity, can influence the optimum reaction temperature. Wilson and Barger[52] showed that the smaller the particle size (less than 1 μm), the longer lifetime of H-SAPO-34 in the MTO reaction. Since the H-SAPO-34 particles used by Bleken et al.[51] are smaller (from 0.2 to 2 μm) than ours, this could explain the observed discrepancy in optimum working temperatures. In our case, the H-SAPO-34 particle size is ∼1−8 μm (Figure S1c), and because of diffusion limitations, the entire crystal volume is, most likely, not fully utilized at 673 K. This reasoning is in line with our in situ microspectroscopy work on large (∼100 × 20 × 20 μm^3) H-ZSM-5 crystals[24−27] and (∼40 × 40 × 40 μm^3) H-SAPO-34 crystals[29,31] during methanol-to-hydrocarbons conversion processes as a function of reaction temperature, although zoning of Al (and Si) may also account for the observed differences.

The product selectivity is dominated by ethylene and propylene, and in general, the sum of both components is higher that 70%. Propylene selectivity is relatively independent of the reaction temperature (25−30%), whereas ethylene selectivity strongly depends on the reaction temperature, from around 40% at low reaction temperatures up to more that 60% for the highest reaction temperature. The selectivity to paraffins is also high, especially at the beginning of the reaction, which can be due to the formation of aromatics inside of the SAPO-34 cages via hydride transfer reactions.[53]

3.3. Operando UV−vis Diffuse Reflectance Spectroscopy. *a. Effect of the Hydrocarbon Pool on Catalyst Activity and Deactivation.* During the catalytic reaction, the catalyst was continuously monitored by operando UV−vis diffuse reflectance spectroscopy. These measurements provide direct insight into the nature and dynamics of distinct hydrocarbon pool species at the different reaction temperatures under study. Figure 2 shows the time-resolved operando UV−vis diffuse reflectance spectra during the induction period of the reaction (indicated in green), at full conversion (indicated in red), when the conversion drops from 100% to 20% (indicated in blue) and finally when the catalyst is completely deactivated (indicated in black).

Clearly, the time-resolved operando UV−vis diffuse reflectance spectra are a complex amalgam of absorption bands with discrete kinetics, and therefore, we have used a multivariate method, named NNMF, for the statistical analysis of the spectroscopic data. More details about these spectroscopic measurements and related analysis using NNMF can be found in our previous work.[28] The results of the analysis are shown in Figure 3.

By applying NNMF, the time-resolved operando UV−vis diffuse reflectance spectra were dissected into two groups of spectra, depicted in Figure 3a, c, e, g, and i, with different kinetic behavior, as illustrated in Figure 3b, d, f, h, and j, which can be interpreted based on the existing literature on band assignments (Table 1).[33,54−69] At low reaction temperatures (573−623 K),

Table 1. Assignments of the Characteristic UV−vis Diffuse Reflectance Absorption Bands Observed on Molecular Sieves during the Methanol-to-Olefins (MTO) Reaction[28,33,54−69]

species	UV−vis band [cm^{-1}]	ref
neutral (methylated) benzenes, the highest wavenumbers corresponding to molecules with the lowest number of − CH_3 groups	36000−39000	33, 55, 61
monoenyl carbocations	33000−34000	54, 63, 59
alkyl-substituted cyclopentenyl carbocations	33000−34000	59
dienyl carbocations	29000−31000	54, 61, 64, 65
low methylated benzene carbocations (up to 4 −CH_3 groups)	29000−31000	28
highly methylated benzene carbocations (5−6 −CH_3 groups)	25000−26000	28, 55−59
methylated naphthalene carbocations	23000−24000	28, 57, 58
neutral polyaromatics	23000−24000	40, 66, 67
phenanthrene and/or anthracene carbocations	16000−17000	28, 57, 58, 68

the *first group of hydrocarbon species* comprises absorption bands at ∼34 000 and ∼26 000 cm^{-1}, which arise from monoenyl[45,59] and highly methylated benzene carbocations[28,55−58] (Table 1). In contrast, at higher reaction temperatures the *first group of hydrocarbon species* is characterized by absorption bands at ∼36 000 and ∼24 500 cm^{-1}, which correspond respectively to neutral aromatics[55,61] and methylated naphthalene carbocations (Table 1).[28,57,58]

To understand the role of this *first group of hydrocarbon species*, the kinetics of these species were compared with the catalytic performance. The analysis shows that the intensity of the first group of hydrocarbon species increases until reaching a maximum at full conversion and then, in general, decreases until it is virtually disappeared when the catalyst deactivates, which suggest that these species are associated with catalyst activity.

The *second group of hydrocarbon species* at low reaction temperatures (573 and 598 K) includes absorption bands at ∼30 000 and ∼24 500 cm^{-1}, which are assigned to low methylated benzene carbocations[28] and methylated naphthalene carbocations,[28,57,58] respectively. By inspecting the kinetics of those species, their contribution increases with increasing time-on-stream. This indicates that the role of this *second group of hydrocarbon species* is closely related to the stage of deactivation of the material. As a consequence, we propose that the role of methylated naphthalene carbocations is blocking the pores of the H-SAPO-34 material, whereas the low methylated benzene carbocations arise as a consequence of demethylation of highly

DOI: 10.1021/acscatal.7b01497
ACS Catal. 2017, 7, 5268−5281

methylated carbocations due to the lack of methanol inside of the H-SAPO-34 material.[70] As mentioned before, and in line with the work of Haw and co-workers,[34] it is postulated that low methylated benzene carbocations are less-active HCP species than highly methylated benzene carbocations, while at the same time more selective toward ethylene.

At higher reaction temperatures (i.e., 623−773 K) the chemistry of the *second group of hydrocarbon species* clearly changes. More specifically, at 623 and 673 K, catalyst deactivation goes along with a broadening of the absorption band at ∼24 500 cm^{-1}, together with the formation of bands at ∼20 000 and ∼16 700 cm^{-1}. This suggests that at these temperatures, the methylated naphthalene carbocations are not the deactivating species, but instead the neutral poly aromatics and phenanthrene/anthracene carbocations deactivates the H-SAPO-34 catalyst material by hindering the diffusion of the reaction products (Table 1). At 773 K, a featureless spectrum is observed, which is due to the formation of more conjugated aromatics, most probably deposited on the external surface. The contribution of this *second group of hydrocarbon species* increases linearly with increasing methanol loading and deactivation of H-SAPO-34 occurs when it reaches a plateau, indicating complete pore blockage by external coke.

On the basis of these observations, we are able to conclude that on H-SAPO-34 the activity and selectivity can be also linked to the formation of hydrocarbon species on the catalyst. Additionally, the chemistry of the hydrocarbon species is fairly sensitive to the reaction temperature, in agreement with our previous results for H-SSZ-13 catalyst.[28] The nature of the active species appears to be very similar for both H-SAPO-34 and H-SSZ-13 (Figure S3 in the Supporting Information). However, the highly methylated benzene carbocations are the dominant active species at higher reaction temperatures (573−623 K) compared to H-SSZ-13 (573−598 K). Looking at the deactivating species, for H-SSZ-13 the contribution of the external coke toward deactivation is higher as compared to H-SAPO-34. The different behavior is, most probably, due to the higher acidity of the H-SSZ-13 material, favoring the formation of more conjugated bulky species (Figure S1c of the Supporting Information). The higher acidity of SSZ-13 is confirmed by the higher desorption temperature of NH_3 (i.e., 685 K)[28] compared to 600 K for SAPO-34 as shown in Figure S3 in the Supporting Information.

b. Effect of the Hydrocarbon Pool on Catalyst Selectivity. Our operando UV−vis diffuse reflectance spectroscopy and NNMF analysis methodology allows the identification of the active and deactivating species during the MTO reaction at different reaction temperatures. The next step was to unravel the origin of the catalyst selectivity during the reaction. Figure 4 plots the measured ethylene-to-propylene ratio for the MTO reaction over H-SAPO-34 with increasing reaction temperature and time-on-stream. Two main features are observed: one at low reaction temperatures (573−623 K) where the ethylene-to-propylene ratio is high at the first stages of the MTO reaction and then decreases and somehow stabilizes. In the second at high reaction temperatures (673−773 K), the ethylene-to-propylene ratio is always increasing with time-on-stream.

Interestingly, these changes in catalyst selectivity patterns correlate with the changes in the nature of the active species. In this way, the group of monoenylic and highly methylated benzene carbocations will be more selective to the formation of propylene, whereas the formation of the group of low methylated benzene carbocations and methylated naphthalene carbocations at higher reaction temperatures (i.e., 673 and 773 K) favors the

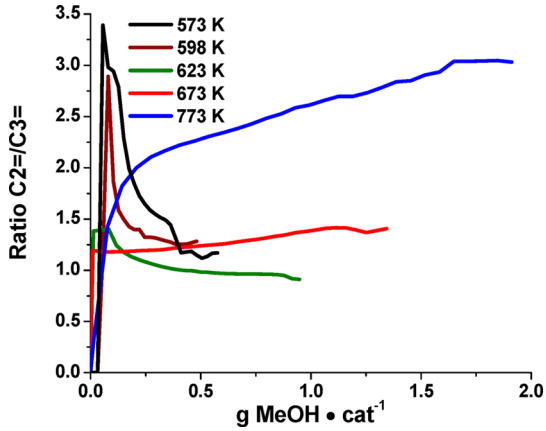

Figure 4. Ethylene-to-propylene ratio calculated from the product composition for the methanol-to-olefin reaction as a function of the methanol throughput over H-SAPO-34.

formation of ethylene. Our results are in line with the studies conducted by Haw et al. on the selectivity of H-SAPO-34.[62] These authors prepared a H-SAPO-34 catalyst containing methylated naphthalene carbocations in the cages and this material yielded a higher amount of ethylene than an analogous material loaded with methylbenzenes.

c. Effect of the Olefins Reactivity on Catalyst Selectivity. If catalyst deactivation was dictated solely by the hydrocarbon pool species, we are unable to determine the origin of the changes in selectivity with time-on-stream. In fact, the evolution of the selectivity at low reaction temperature (573−623 K) drastically changes at the beginning of the reaction, ranging from a catalyst system very selective toward ethylene to one which is more selective toward propylene. The secondary reaction of olefins might account for these changes in the selectivity with increasing time-on-stream. To evaluate this effect, we have performed a set of experiments, feeding a mixture of ethylene, propylene, and water, mimicking the formation of reaction products during the MTO reaction. During these experiments, the hydrocarbons formed on the catalysts and changes in olefin composition were analyzed by operando UV−vis diffuse reflectance spectroscopy and online GC, respectively.

Figure 5a,b show the incorporation of ethylene and propylene into the catalyst as hydrocarbon pool species, respectively. The composition of the gas stream after going through the catalyst bed is also plotted in Figure S4 of the Supporting Information. The results show that both olefins are incorporated into the hydrocarbon pool but at different levels. The incorporation of propylene into the hydrocarbon pool is, in general, ∼2−3 times higher than for ethylene. As an example, at 598 K the incorporation of ethylene and propylene is around 20 and 60 mol % after 10 min on stream, respectively. Based on these experiments we suggest that the changes in catalyst selectivity with increasing time-on-stream are closely related to the incorporation of olefins into the hydrocarbon pool.

In order to evaluate the effect of the hydrocarbon species formed by olefins, the MTO reaction were performed on the SAPO-34 catalyst after olefin feeding. The operando UV−vis diffuse reflectance spectra recorded at the end of olefins/water feeding experiments and during the MTO reaction are presented in Figure 6.

During olefins/water feeding the development of the absorption bands in the operando UV−vis diffuse reflectance spectra at ∼36 000, ∼26 000−23 000, ∼20 000, and ∼16 000

DOI: 10.1021/acscatal.7b01497
ACS Catal. 2017, 7, 5268−5281

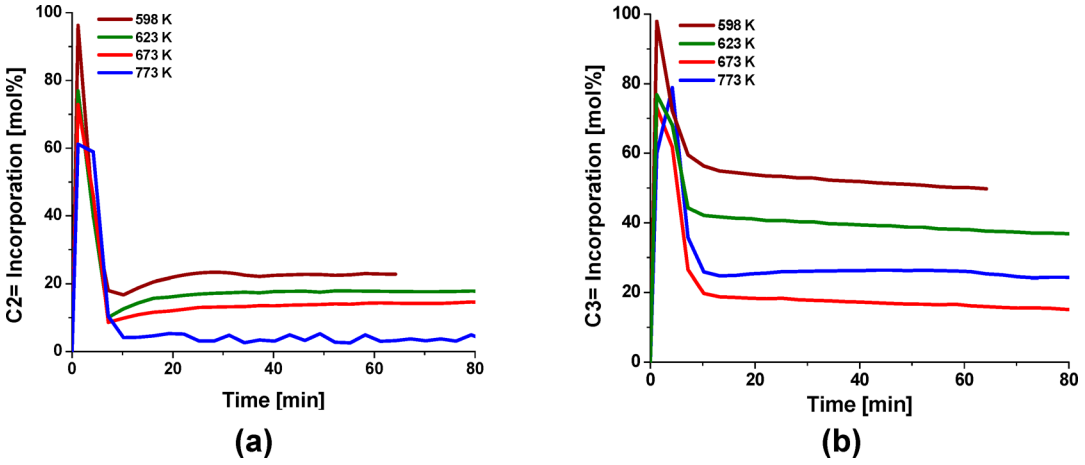

Figure 5. (a) Incorporation of $C_{2=}$ and (b) incorporation of $C_{3=}$ during the $C_{2=}/C_{3=}/H_2O$ feeding experiments at different reaction temperatures vs time-on-stream for a H-SAPO-34 catalyst.

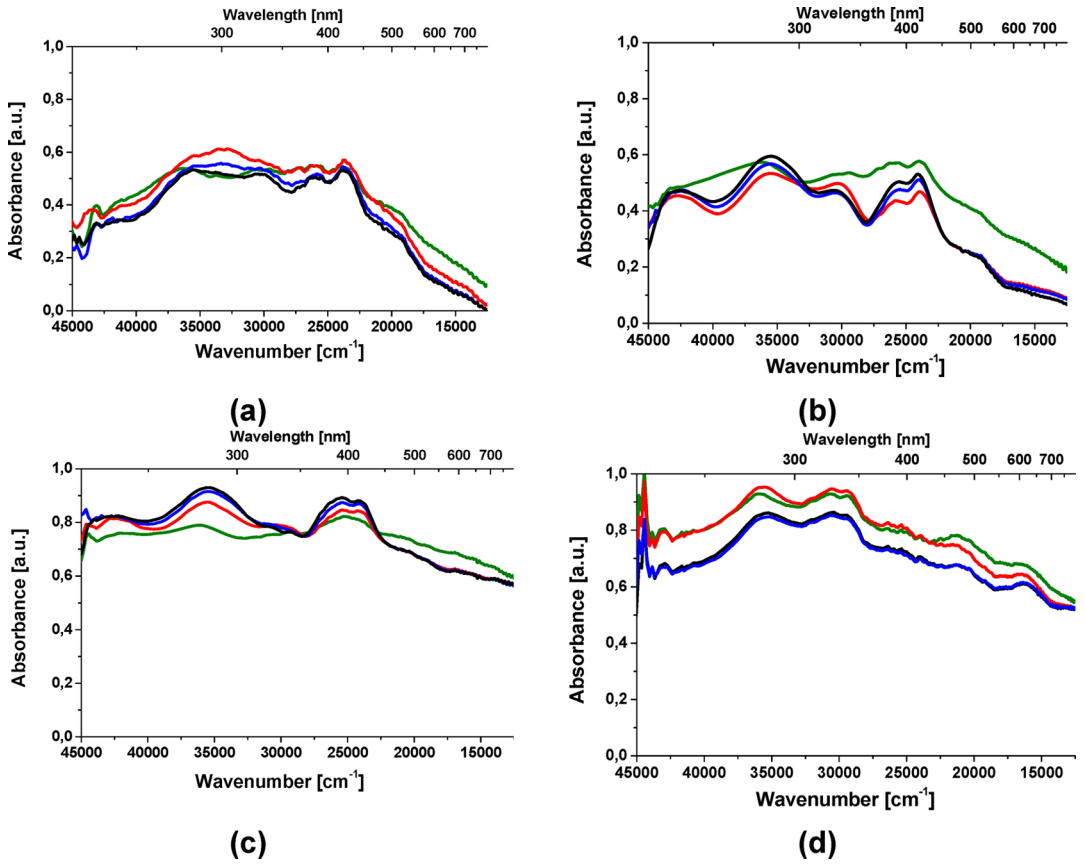

Figure 6. Operando UV−vis diffuse reflectance spectra recorded at (a) at 598 K; (b) 623 K; (c) 673 K; and (d) 773 K. The green spectrum corresponds to the end of the $C_{2=}/C_{3=}/H_2O$ feeding experiments; the red spectrum relates to the full MeOH conversion; the blue spectrum indicates deactivation of H-SAPO-34, while the black spectrum corresponds to catalyst deactivation.

cm^{-1} is observed. These absorption bands can be interpreted on the basis of Table 1, which summarizes the spectral assignment of these and other absorption bands based on the literature.[28,33,54−69]

On the basis of this analysis, the formation of the neutral and charged aromatics with a different degree of conjugation and methylation degree is observed, i.e., neutral benzenes, low and highly methylated benzene carbocations, methylated naphthalene carbocations, and phenanthrene/anthracene carbocations. Therefore, olefins and mainly propylene contribute to the formation not only of HCP, that is, methylated benzene and naphthalene carbocations, but also of more conjugated aromatics, such as phenanthrene and anthracene carbocations. Additionally, the development of background absorption in the operando UV−vis diffuse reflectance spectra indicates the formation of external coke from the olefins. Further evidence for this observation comes from our previous work involving operando UV−vis and confocal fluorescence microspectroscopy on large H-SAPO-34 and H-ZSM-5 crystals.[24−27,29,31]

DOI: 10.1021/acscatal.7b01497
ACS Catal. 2017, 7, 5268−5281

The start of the methanol flow during the MTO reaction does not cause changes of the chemistry of the species already formed during olefins feeding experiments because the position of the absorption bands for the UV−vis spectra at full MeOH conversion (red color) does not change. However, for low reaction temperatures (i.e., 598 and 623 K), the formation of a new UV−vis band at ∼33 650 cm^{-1} is observed. This band can be either assigned to monoenyl carbocations[54,63] or alkyl-substituted cyclopentenyl carbocations (Table 1).[33,40] Since we do not detect this absorption band during the olefins feeding experiments, this band could be ascribed to an active hydrocarbon pool species.

To understand the effect of the formation of hydrocarbon deposits on the catalyst lifetime, the methanol throughput during a normal MTO measurement and after olefins reaction was compared and summarized in Table 2. The stability of H-SAPO-34 during the MTO reaction after the prefeeding the catalyst with olefins and water is ∼2 times lower in comparison to the normal MTO reaction (Table 2).

Table 2. Stability of H-SAPO-34 during the MTO Reactions Performed at Normal Conditions and after the Pre-Feeding the Catalyst with Ethylene, Propylene, and Water

	g MeOH $g{\cdot}cat^{-1}$ during the MTO reaction	
temperature [K]	normal conditions	$C_{2=}/C_{3=}/H_2O$ prefeeding
598 K	0.53	0.33
623 K	0.98	0.52
673 K	1.39	0.38
773 K	2.1	1.45

This indicates once more that together with the incorporation of propylene and ethylene into the hydrocarbon pool species, they also contribute to the formation of deactivating hydrocarbon deposits. For every reaction temperature, the feeding time corresponds to the time of the normal MTO reaction (Figure 1). With respect to the operando UV−vis diffuse reflectance spectra after olefins feeding, the level of the background intensity increases with increasing reaction temperature. More specifically, the absorbance of the background increases from 0.15 to 0.60 for the reaction temperature of 598 and 773 K, respectively. It points toward the fact that the higher the reaction temperature, the higher the amount of coke is formed.

However, we cannot rule out here the role of thermodynamics, which can have an influence on the product selectivity of the MTO reaction. This was already reported by Wilson and Barger.[52] For a more precise understanding whether thermodynamics can rule the observed product composition, we have applied the HSC Chemistry Software (Outotec) for calculating the ethylene-to-propylene ratio in the range of applied reaction temperatures. The result is summarized in Figure S5 in the Supporting Information. Indeed, in accordance with the thermodynamic equilibrium, ethylene becomes dominant when the reaction temperature increases, which is in line with the high reaction temperatures (i.e., 673−773 K).

3.4. Further Insights into the Methanol-to-Olefins Mechanism. In order to obtain further insights into the methanol-to-olefins mechanism, we have performed two additional experiments, in which we have switched on and off the methanol flow and at the same time varied the reaction temperature, while continuously measuring the operando UV−vis diffuse reflectance spectra as well as the formation of reaction products. The first of these experiment was conducted at lower reaction temperatures (i.e., between 523 and 573 K), and the results are summarized in Figure 7, which shows the amount of detected reaction products, the recorded time-resolved operando UV−vis diffuse reflectance spectra, and the reaction temperature sequence program applied.

At a reaction temperature of 523 K, no UV−vis absorption bands and no reaction products were detected. Indeed, this temperature is too low to initiate the creation of the hydrocarbon pool in H-SAPO-34. When the reaction temperature was increased up to 543 K, the formation of the absorption band at ∼26 000 cm^{-1} was detected, which is associated with the formation of hydrocarbon pool species, that is, highly methylated benzene carbocations (Table 1). At the same time, the formation of the reaction products started (Figure 7a), and an absorption band at ∼29 000 cm^{-1} emerges, which is, most probably, related to the formation of low methylated benzene carbocations (Figure 7b, Table 1). Demethylation and formation of the reaction products still continued after the methanol flow was stopped. More specifically, the absorption band for the low methylated benzene carbocations became more distinct and even shifted to higher wavenumbers (i.e., ∼ 30 000 cm^{-1}), which is attributed to the further demethylation of benzene carbocations. When the H-SAPO-34 catalyst was brought up to a reaction temperature of 573 K, the reaction products started to form again. A shift of the absorption band from ∼26 000 to ∼25 000 cm^{-1} is observed, which can be indicative for the formation of methylated naphthalene carbocations. This can be a result of the condensation of low methylated benzene carbocations after switching off the methanol flow.

In order to prove the envisaged deactivation mechanism—at lower reaction temperatures (i.e., at 573 and 598 K), where methylated naphtalene carbocations are found to be the deactivating species, and follow the mechanism of the MTO reaction at higher reaction temperatures (i.e., 623−773 K), where the same species are detected to be the active—we have conducted a second additional experiment. In this experiment, first methanol was flowed over the catalyst at 573 K, followed by a switching off of the methanol at the same temperature, followed by a further heating of the catalyst up to a reaction temperature of 623 K. During the switch off of methanol, both the product formation and operando UV−vis diffuse reflectance spectra have been continuously monitored. The results of this additional experiment are summarized in Figure 8.

After the start of the methanol flow at 573 K, the UV−vis bands typical for highly methylated benzene carbocations (∼26 000 cm^{-1}) and monoenyl carbocations (∼33 650 cm^{-1}) appear (Table 1), proving that these carbocations are the active species at lower reaction temperatures (i.e., 573 K). The absorption band for low methylated benzene carbocations (∼29 000 cm^{-1}) is also observed as a consequence of demethylation reactions. When the methanol flow was stopped (i.e., the orange colored spectra in Figure 8), the formation of olefins slows, and the UV−vis band shifts from ∼26 000 to ∼25 000 cm^{-1}, indicating the presence of methylated naphthalene carbocations (Table 1). These species play the role of deactivating species at low reaction temperature. In order to confirm that at higher reaction temperatures these hydrocarbon species are indeed the active species, the H-SAPO-34 catalyst was heated up to 623 K. Then, as it can be concluded from Figure 8a, the reaction products start to form (again). This formation of propylene and ethylene is accompanied by a slight shift of the absorption band at ∼25 000 cm^{-1} to lower wavenumbers, which

DOI: 10.1021/acscatal.7b01497
ACS Catal. 2017, 7, 5268−5281

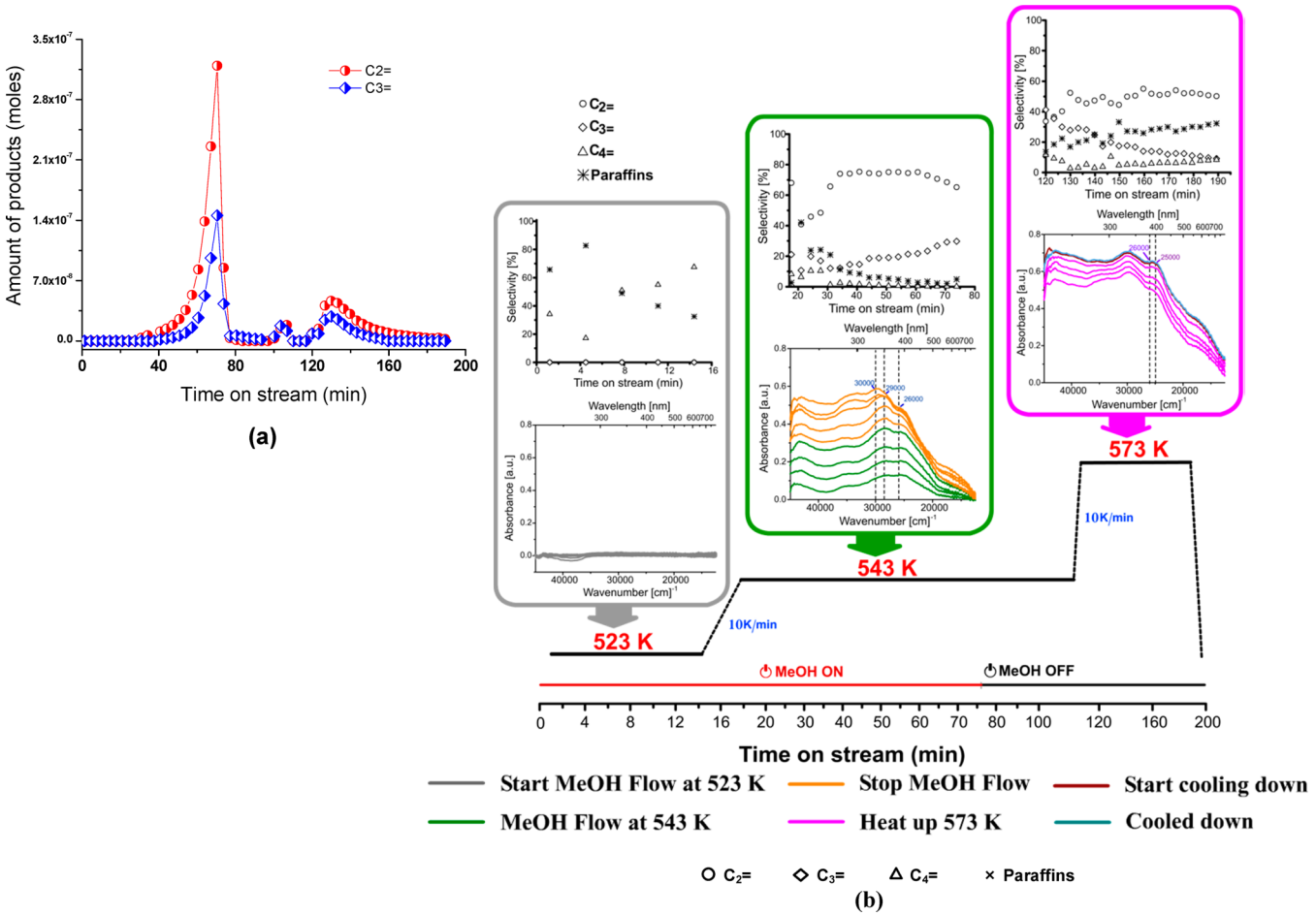

Figure 7. (a) Product composition and (b) selectivity and operando UV−vis diffuse reflectance spectra over H-SAPO-34: at 523 K (in gray) and 543 K (in green) during methanol flow; at 543 K during a stop of the methanol flow and flushing with He (in orange); after heating the catalyst up to 573 K, and holding the material at 573 K (in pink), during cooling to room temperature (in brown) and finally measured at room temperature (in blue).

is a sign of demethylation of naphthalene carbocations (Table 1). On the other hand, the typical UV−vis absorption bands for anthracene and phenanthrene carbocations are also detected at 623 K, which is associated with the formation of hydrocarbon deposits. The formation of hydrocarbon species that are deactivating and blocking the catalyst micropores at lower reaction temperatures, while become the active HCP species at higher reaction temperatures has also been observed for other small-pore zeolites. More specifically, the role of 1-methylnapthalene during MTO in framework structure DDR is deactivating at 623 K, while becoming an active HCP species at 723 K.[71] On the other hand, in line with the earlier work of Hereijgers and co-workers,[70] some of the spectroscopically observed hydrocarbon species may not be accessible for reaction with incoming species, thereby influencing both activity and selectivity.

4. CONCLUSIONS

This study was directed toward the understanding of the parameters ruling olefin selectivity and catalyst deactivation during MTO conversion over H-SAPO-34. We have found that several factors dictate the ethylene/propylene selectivity. First of all, the ethylene-to-propylene ratio decreases for the temperature window of 573−623 K and increases when the reaction temperature was increased up to 773 K. Second, at lower reaction temperatures (i.e., 573−623 K), the selectivity is ruled by the high degree of incorporation of olefins, mainly propylene, into the hydrocarbon pool. The nature and dynamics of active and deactivating species with increasing reaction temperature were determined by a detailed analysis of the time-resolved operando UV−vis diffuse reflectance spectra with non-negative matrix factorization. It was concluded that the active hydrocarbon pool species at 573 and 598 K are mainly highly methylated benzene carbocations and monoenyl carbocations, while at 623 K low methylated benzene carbocations and methylated naphthalene carbocations become the more dominant hydrocarbon pool species. Furthermore, at reaction temperatures of 673 and 773 K, only methylated naphthalene carbocations are observed, while also some neutral aromatics are detected. The changes in hydrocarbon pool species also influence the olefin selectivity. More specifically, the group of monoenylic and highly methylated benzene carbocations are more selective to the formation of propylene, whereas the formation of the group of low methylated benzene carbocations and methylated naphthalene carbocations at higher reaction temperatures (i.e., 673 and 773 K) favors the formation of ethylene.

At 573 and 598 K, catalyst deactivation occurs due to the pore filling with these methylated naphthalene carbocations. At temperatures between 623 and 773 K, catalyst deactivation occurs due to the formation of neutral poly aromatics and phenanthrene/anthracene carbocations on the external surface. These species contribute the most to the catalyst behavior with

DOI: 10.1021/acscatal.7b01497
ACS Catal. 2017, 7, 5268−5281

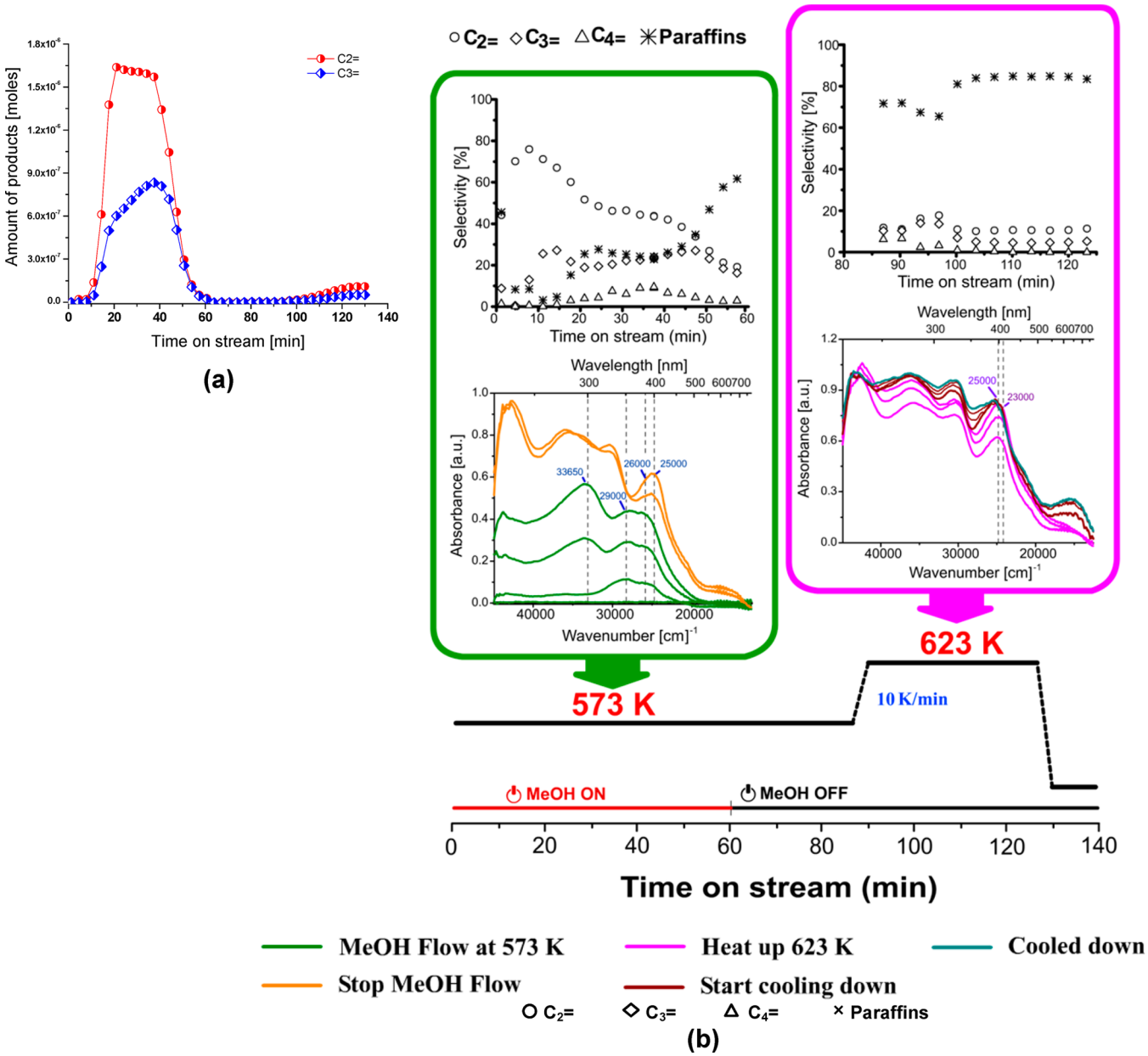

Figure 8. (a) Product composition and (b) selectivity and operando UV−vis diffuse reflectance spectra of H-SAPO-34 recorded: at 573 K (in green) during methanol flow; at 573 K during stop of methanol flow and flushing with He (in orange); at heating up and holding the catalyst up at 623 K (in pink) and during cooling to room temperature (in brown) and finally at room temperature (in blue).

increasing reaction temperature. The formation of bulkier deactivating species with increasing temperature also seems to have an impact on the higher ethylene-to-propylene ratio. When comparing SAPO-34 with the zeolite analogous SSZ-13, the nature of the active and deactivating species are very similar, although in SAPO-34 the hydrocarbon species causing activity are more stable at higher temperatures. The different behavior is, most probably, due to the higher acidity of the H-SSZ-13 material, favoring the formation of more conjugated and bulky hydrocarbon species.

■ ASSOCIATED CONTENT

Supporting Information

The Supporting Information is available free of charge on the ACS Publications website at DOI: 10.1021/acscatal.7b01497.

XRD pattern, SEM image, ammonia-TPD profile, Ar adsorption and desorption isotherm, and propylene-to-ethylene ratio incorporated to hydrocarbon pool vs ethylene to propylene ratio in the eluent for H-SAPO-34 as well as a function of reaction temperature (PDF)

■ AUTHOR INFORMATION

Corresponding Authors

*B.M.W.: e-mail: b.m.weckhuysen@uu.nl; tel.: +31 30 253 4328.
*J.R.-M.: e-mail: javier.ruizmartinez@akzonobel.com; tel: +31 62 273 6379.

ORCID

M. Mokhtar: 0000-0002-0594-7207
B. M. Weckhuysen: 0000-0001-5245-1426

DOI: 10.1021/acscatal.7b01497
ACS Catal. 2017, 7, 5268−5281

Notes

The authors declare no competing financial interest.

■ ACKNOWLEDGMENTS

This research work is funded by The Netherlands Research School Combination-Catalysis (NRSC-C) and the Deanship of Scientific Research (DSR) of King Abdulaziz University, Jeddah under grant number (T-002-431). The authors gratefully acknowledge DSR for technical and financial support. Javier Ruiz-Martinez and Florian Meirer also acknowledge CW-NWO for their VENI and VIDI grant, respectively. Pascal Wijten (Utrecht University, UU) is acknowledged for the assistance with GC-MS analysis of the retained hydrocarbons, while Abhishek Dutta Chowdhury (UU) is thanked for valuable discussions.

■ REFERENCES

(1) Tian, P.; Wei, Y. X.; Ye, M.; Liu, Z. M. *ACS Catal.* **2015**, *5*, 1922−1938.
(2) Ilias, S.; Bhan, A. *ACS Catal.* **2013**, *3*, 18−31.
(3) Olsbye, U.; Svelle, S.; Lillerud, K. P.; Wei, Z. H.; Chen, Y. Y.; Li, J. F.; Wang, J. G.; Fan, W. B. *Chem. Soc. Rev.* **2015**, *44*, 7155−7176.
(4) Vogt, E. T. C.; Whiting, G. T.; Dutta Chowdhury, A.; Weckhuysen, B. M. *Adv. Catal.* **2015**, *58*, 143−314.
(5) Olsbye, U.; Svelle, S.; Bjorgen, P.; Beato, P.; Janssens, T. V. W.; Joensen, F.; Bordiga, S.; Lillerud, K. P. *Angew. Chem., Int. Ed.* **2012**, *51*, 5810−5831.
(6) Stöcker, M. *Microporous Mesoporous Mater.* **1999**, *29*, 3−48.
(7) Dahl, I. M.; Kolboe, S. *Catal. Lett.* **1993**, *20*, 329−336.
(8) Lercher, J. A. *ACS Cent. Sci.* **2015**, *1*, 350−351.
(9) Comas-Vives, A.; Valla, M.; Copéret, C.; Sautet, P. *ACS Cent. Sci.* **2015**, *1*, 313−319.
(10) Liu, Y.; Müller, S.; Berger, D.; Jelic, J.; Reuter, K.; Tonigold, M.; Sanchez-Sanchez, M.; Lercher, J. A. *Angew. Chem., Int. Ed.* **2016**, *55*, 5723−5726.
(11) Dutta Chowdhury, A.; Houben, K.; Whiting, G. T.; Mokhtar, M.; Asiri, A. M.; Al-Thabaiti, S. A.; Basahel, S. N.; Baldus, M.; Weckhuysen, B. M. *Angew. Chem., Int. Ed.* **2016**, *55*, 15840−15845.
(12) Wang, C. M.; Wang, Y. D.; Xie, Z. K. *J. Catal.* **2013**, *301*, 8−19.
(13) Wang, S.; Chen, Y.; Wei, Z.; Qin, Z.; Chen, J.; Ma, H.; Dong, M.; Li, J.; Fan, W.; Wang, J. *J. Phys. Chem. A* **2014**, *118*, 8901−8910.
(14) Van Speybroeck, V.; De Wispelaere, K.; Van der Mynsbrugge, J.; Vandichel, M.; Hemelsoet, K.; Waroquier, M. *Chem. Soc. Rev.* **2014**, *43*, 7326−7357.
(15) Muller, S.; Liu, Y.; Kirchberger, F. M.; Tonigold, M.; Sanchez-Sanchez, M.; Lercher, J. A. *J. Am. Chem. Soc.* **2016**, *138*, 15994−16003.
(16) Hwang, A.; Kumar, M.; Rimer, J. D.; Bhan, A. *J. Catal.* **2017**, *346*, 154−160.
(17) Hwang, A.; Prieto-Centurion, D.; Bhan, A. *J. Catal.* **2016**, *337*, 52−56.
(18) Ilias, S.; Bhan, A. *J. Catal.* **2014**, *311*, 6−16.
(19) Dai, W.; Dyballa, M.; Wu, G.; Li, L.; Guan, N.; Hunger, M. *J. Phys. Chem. C* **2015**, *119*, 2637−2645.
(20) Song, W.; Marcus, D. M.; Fu, H.; Ehresmann, J. O.; Haw, J. F. *J. Am. Chem. Soc.* **2002**, *124*, 3844−3845.
(21) Dai, W.; Wang, C.; Dyballa, M.; Wu, G.; Guan, N.; Li, L.; Xie, L.; Hunger, M. *ACS Catal.* **2015**, *5*, 317−326.
(22) Wang, W.; Hunger, M. *Acc. Chem. Res.* **2008**, *41*, 895−904.
(23) Wang, C.; Chu, Y.; Zheng, A.; Xu, J.; Wang, Q.; Gao, P.; Qi, G.; Gong, Y.; Deng, F. *Chem. - Eur. J.* **2014**, *20*, 12432−12443.
(24) Mores, D.; Stavitski, E.; Kox, M. H. F.; Kornatowski, J.; Olsbye, U.; Weckhuysen, B. M. *Chem. - Eur. J.* **2008**, *14*, 11320−11327.
(25) Mores, D.; Kornatowski, J.; Olsbye, U.; Weckhuysen, B. M. *Chem. - Eur. J.* **2011**, *17*, 2874−2884.
(26) Hofmann, J. P.; Mores, D.; Aramburo, L. R.; Teketel, S.; Rohnke, M.; Janek, J.; Olsbye, U.; Weckhuysen, B. M. *Chem. - Eur. J.* **2013**, *19*, 8533−8542.
(27) Nordvang, E. C.; Borodina, E.; Ruiz-Martinez, J.; Fehrmann, R.; Weckhuysen, B. M. *Chem. - Eur. J.* **2015**, *21*, 17324−17335.
(28) Borodina, E.; Meirer, F.; Lezcano-González, I.; Mokhtar, M.; Asiri, A. M.; Al-Thabaiti, S. A.; Basahel, S. N.; Ruiz-Martínez, J.; Weckhuysen, B. M. *ACS Catal.* **2015**, *5*, 992−1003.
(29) Qian, Q.; Ruiz-Martínez, J.; Mokhtar, M.; Asiri, A. M.; Al-Thabaiti, S. A.; Basahel, S. N.; Weckhuysen, B. M. *ChemCatChem* **2014**, *6*, 772−783.
(30) Qian, Q.; Vogt, C.; Mokhtar, M.; Asiri, A. M.; Al-Thabaiti, S. A.; Basahel, S. N.; Ruiz-Martínez, J.; Weckhuysen, B. M. *ChemCatChem* **2014**, *6*, 3396−3408.
(31) De Wispelaere, K.; Wondergem, C. S.; Ensing, B.; Hemelsoet, K.; Meijer, E. J.; Weckhuysen, B. M.; Van Speybroeck, V.; Ruiz-Martinez, J. *ACS Catal.* **2016**, *6*, 1991−2002.
(32) Arstad, B.; Kolboe, S. *J. Am. Chem. Soc.* **2001**, *123*, 8137−8138.
(33) Wulfers, M. J.; Jentoft, F. C. *ACS Catal.* **2014**, *4*, 3521−3532.
(34) Sassi, A.; Wildman, M. A.; Ahn, H. J.; Prasad, P.; Nicholas, J. B.; Haw, J. F. *J. Phys. Chem. B* **2002**, *106*, 2294−2303.
(35) Chen, D.; Rebo, H. P.; Moljord, K.; Holmen, A. *Ind. Eng. Chem. Res.* **1997**, *36*, 3473−3479.
(36) Chen, D.; Moljord, K.; Fuglerud, T.; Holmen, A. *Microporous Mesoporous Mater.* **1999**, *29*, 191−203.
(37) Sun, X.; Mueller, S.; Shi, H.; Haller, G. L.; Sanchez-Sanchez, M.; van Veen, A. C.; Lercher, J. A. *J. Catal.* **2014**, *314*, 21−31.
(38) Wu, X.; Anthony, R. G. *Appl. Catal., A* **2001**, *218*, 241−250.
(39) Li, Z.; Martínez-Triguero, J.; Concepción, P.; Yu, J.; Corma, A. *Phys. Chem. Chem. Phys.* **2013**, *15*, 14670−14680.
(40) Park, J. W.; Lee, J. Y.; Kim, K. S.; Hong, S. B.; Seo, G. *Appl. Catal., A* **2008**, *339*, 36−44.
(41) Li, J.; Wei, Y.; Chen, J.; Xu, S.; Tian, P.; Yang, X.; Li, B.; Wang, J.; Liu, Z. *ACS Catal.* **2015**, *5*, 661−665.
(42) Pop, G.; Ganea, R.; Ivanescu, D.; Ignatescu, G.; Boeru, R.; Birjega, R. Patent WO2000/041986, 1999.
(43) Guisnet, M.; Gilson, J.-P. *Zeolites for Cleaner Technologies*; Guisnet, M., Gilson, J.-P., Hutchings, G. J., Eds.; Imperial College Press: London, 2002; Vol. 3, pp 1−388.
(44) Lee, D. D.; Seung, H. S. *Nature* **1999**, *401*, 788−791.
(45) Lee, D. D.; Seung, H. S. In *Advances in Neural Information Processing Systems 13: Proceedings of the 2000 Conference*; Leen, T. K., Dietterich, T. G., Tresp, V., Eds.; MIT Press: Cambridge, MA, 2000; pp 556−562.
(46) International Zeolite Association. www.iza-online.org.
(47) Jeon, H.-Y.; Shin, C.-H.; Jung, H. J.; Hong, S. B. *Appl. Catal., A* **2006**, *305*, 70−78.
(48) Zhu, Q.; Kondo, J. N.; Tatsumi, T.; Inagaki, S.; Ohnuma, R.; Kubota, Y.; Shimodaira, Y.; Kobayashi, H.; Domen, K. *J. Phys. Chem. C* **2007**, *111*, 5409−5415.
(49) Martins, G. V. A.; Berlier, G.; Bisio, C.; Coluccia, S.; Pastore, H. O.; Marchese, L. *J. Phys. Chem. C* **2008**, *112*, 7193−7200.
(50) Vomscheid, R.; Briend, M.; Peltre, M.-J.; Barthomeuf, D.; Man, P. P. *J. Chem. Soc., Faraday Trans.* **1995**, *91*, 3281−3284.
(51) Bleken, F.; Bjørgen, M.; Palumbo, L.; Bordiga, S.; Svelle, S.; Lillerud, K.-P.; Olsbye, U. *Top. Catal.* **2009**, *52*, 218−228.
(52) Wilson, S.; Barger, P. *Microporous Mesoporous Mater.* **1999**, *29*, 117−126.
(53) Marchi, A. J.; Froment, G. F. *Appl. Catal.* **1991**, *71*, 139−152.
(54) Kiricsi, I.; Förster, H.; Tasi, G.; Nagy, J. B. *Chem. Rev.* **1999**, *99*, 2085−2114.
(55) Bjørgen, M.; Bonino, F.; Kolboe, S.; Lillerud, K.-P.; Zecchina, A.; Bordiga, S. *J. Am. Chem. Soc.* **2003**, *125*, 15863−15868.
(56) Bjørgen, M.; Bonino, F.; Arstad, B.; Kolboe, S.; Lillerud, K.-P.; Zecchina, A.; Bordiga, S. *ChemPhysChem* **2005**, *6*, 232−235.
(57) Van Speybroeck, V.; Hemelsoet, K.; De Wispelaere, K.; Qian, Q.; Van der Mynsbrugge, J.; De Sterck, B.; Weckhuysen, B. M.; Waroquier, M. *ChemCatChem* **2013**, *5*, 173−184.
(58) Hemelsoet, K.; Qian, Q.; De Meyer, T.; De Wispelaere, K.; De Sterck, B.; Weckhuysen, B. M.; Waroquier, M.; Van Speybroeck, V. *Chem. - Eur. J.* **2013**, *19*, 16595−16606.
(59) Wulfers, M. J.; Jentoft, F. C. *J. Catal.* **2013**, *307*, 204−213.

DOI: 10.1021/acscatal.7b01497
ACS Catal. 2017, 7, 5268−5281

(60) Haw, J. F.; Nicholas, J. B.; Song, W.; Deng, F.; Wang, Z.; Xu, T.; Heneghan, C. S. *J. Am. Chem. Soc.* **2000**, *122*, 4763−4775.
(61) Dai, W.; Wu, G.; Li, L.; Guan, N.; Hunger, M. *ACS Catal.* **2013**, *3*, 588−596.
(62) Song, W.; Fu, H.; Haw, J. F. *J. Phys. Chem. B* **2001**, *105*, 12839−12843.
(63) Förster, H.; Kiricsi, I.; Tasi, G.; Hannus, I. *J. Mol. Struct.* **1993**, *296*, 61−67.
(64) Kiricsi, I.; Förster, H. *J. Chem. Soc., Faraday Trans. 1* **1988**, *84*, 491−499.
(65) Demidov, A. V.; Davydov, A. A. *Mater. Chem. Phys.* **1994**, *39*, 13−20.
(66) Dai, W.; Scheibe, M.; Guan, N.; Li, L.; Hunger, M. *ChemCatChem* **2011**, *3*, 1130−1133.
(67) Dai, W.; Scheibe, M.; Li, L.; Guan, N.; Hunger, M. *J. Phys. Chem. C* **2012**, *116*, 2469−2476.
(68) Palumbo, L.; Bonino, F.; Beato, P.; Bjørgen, M.; Zecchina, A.; Bordiga, S. *J. Phys. Chem. C* **2008**, *112*, 9710−9716.
(69) Dahl, I. M.; Wendelbo, R.; Andersen, A.; Akporiaye, D.; Mostad, H.; Fuglerud, T. *Microporous Mesoporous Mater.* **1999**, *29*, 159−171.
(70) Hereijgers, B. P. C.; Bleken, F.; Nilsen, M. H.; Svelle, S.; Lillerud, K.-P.; Bjørgen, M.; Weckhuysen, B. M.; Olsbye, U. *J. Catal.* **2009**, *264*, 77−87.
(71) Goetze, J.; Meirer, F.; Yarulina, I.; Gascon, J.; Kapteijn, F.; Ruiz-Martinez, J.; Weckhuysen, B. M. *ACS Catal.* **2017**, *7*, 4033−4046.

DOI: 10.1021/acscatal.7b01497
ACS Catal. 2017, 7, 5268−5281